

# A molecular tweezers-like calix[4]arene based alkaline earth metal cation ( $\text{Ca}^{2+}$ , $\text{Sr}^{2+}$ & $\text{Ba}^{2+}$ ) chemosensor and its imaging in living cells and zebrafish

Jun-An Fang,<sup>†,‡</sup> Jiang-Lin Zhao,<sup>\*†</sup> Xian Liao,<sup>‡</sup> Xi Zeng,<sup>\*‡</sup> Kai Chen,<sup>‡</sup> Xiao-Yuan Wei,<sup>†</sup> Shao-Bo Su,<sup>†</sup> Qing-Ying Luo,<sup>†</sup> Carl Redshaw<sup>§</sup> and Zongwen Jin<sup>\*†</sup>

<sup>†</sup>Institute of Biomedical & Health Engineering, Shenzhen Institutes of Advanced Technology, Chinese Academy of Sciences, 1068 Xueyuan Avenue, Shenzhen 518055, China.

<sup>‡</sup>Key Laboratory of Macrocyclic and Supramolecular Chemistry of Guizhou Province; School of Chemistry and Chemical engineering, Guizhou University, Guiyang 550025, China.

<sup>‡</sup>Jiangsu Collaborative Innovation Center of Atmospheric Environment and Equipment Technology, Jiangsu Key Laboratory of Atmospheric Environment Monitoring and Pollution Control, School of Environmental Science and Engineering, Nanjing University of Information Science & Technology, Nanjing 210044, China.

<sup>§</sup>Dept. of Chemistry & Biochemistry, University of Hull, Hull HU6 7RX, U.K.

**KEYWORDS:** Calix[4]arene, Chemosensor, Alkaline earth metal ions, Synergistic effect, Molecular tweezers

---

**ABSTRACT:** Although alkaline earth metal cations play an important role in our daily life, little attention has been paid to the field of fast quantitative analysis of their content due to a lack of satisfactory precision, and a fast and convenient means of detection. In this study, we have designed a set of molecular tweezers based on the calix[4]arene chemosensor **L**, which was found to exhibit high selectivity and sensitivity towards  $\text{Ca}^{2+}$ ,  $\text{Sr}^{2+}$  and  $\text{Ba}^{2+}$  (by UV-vis and fluorescence methods) with low detection limits of the order of  $10^{-7}$  to  $10^{-8}$  M and high association constants (of the order of  $10^6$ ). More significantly, sensor **L** not only can recognize  $\text{Ca}^{2+}$ ,  $\text{Sr}^{2+}$  and  $\text{Ba}^{2+}$ , but can also further discriminate between these three cations via the differing red shifts in their UV-vis spectra (560 nm for **L**• $\text{Ca}^{2+}$ , 570 nm for **L**• $\text{Sr}^{2+}$  and 580 nm for **L**• $\text{Ba}^{2+}$  complex) which is attributed to their different atomic radii. A rare synergistic effect for the recognition mechanism has been demonstrated by  $^1\text{H}$  NMR spectroscopic titration. Sensor **L** constructed a high shielding field by the cooperation of Tris with alkaline earth metal ion after complex. Additionally, the presence of acetoxymethyl group in sensor **L** results in enhancement of cell permeability and as a consequence, sensor **L** exhibited excellent sensing and imaging (*in vivo*) in living cells and in Zebrafish.

---

## INTRODUCTION

Calcium (Ca), the fifth most abundant element in the human body, is necessary for both our reproduction and growth.<sup>1</sup> The significance of  $\text{Ca}^{2+}$  cations in biology results from changes in their concentration that can directly influence normal body and physiological functions. For example, dysregulation of intracellular  $\text{Ca}^{2+}$  concentration is implicated in the pathogenesis of Alzheimer's disease.<sup>2</sup> Strontium (Sr) is usually very toxic owing to its radioactivity ( $^{90}\text{Sr}$ , half-life of 28.8 years) and finds use in the manufacture of "dirty bomb".<sup>3</sup> Given its high water solubility, an excess of Sr has recognized as a pollutant in drinking water and is detrimental to the aquatic environment. Given this, highly sensitive and rapid detection of  $\text{Sr}^{2+}$  in groundwater will aid clean-up operations and help prevent public health hazard. Furthermore, barium (Ba), a heavier group II element, is also essential at trace levels.<sup>4</sup> However, increased levels of  $\text{Ba}^{2+}$  in the body can result in acute gastroenteritis, muscular paralysis, respiratory failure, loss of deep reflexes, and on occasion even death.<sup>5</sup>

Given these issues, fast and sensitive technologies are required to monitor fluctuations in the concentrations of these

alkaline earth metal cations. Among various detection methods, chemosensor assays have become the most popular method for monitoring important biological events, both *in vitro* and *in vivo*, due to desirable features such as high selectivity, high sensitivity, real-time imaging and facile manipulation.<sup>6</sup> Numerous  $\text{Ca}^{2+}$  chemosensors<sup>7</sup> have been developed since the introduction of small-molecule fluorescent indicators by Tsien *et al* in the mid-1980s.<sup>8</sup> In contrast, little attention has been paid to  $\text{Ba}^{2+}$ <sup>9</sup> and  $\text{Sr}^{2+}$  chemosensors, especially for  $\text{Sr}^{2+}$ ; only 5  $\text{Sr}^{2+}$  sensors have been reported.<sup>10</sup> Moreover, little is known about the simultaneous detection of these three alkaline earth metals ( $\text{Ca}^{2+}$ ,  $\text{Sr}^{2+}$  and  $\text{Ba}^{2+}$ ).

To broaden the available sensing of these alkaline earth metal cations, we have designed herein a set of molecular tweezers based on the calix[4]arene chemosensor (**L**): two vinyl pyridinium motifs are appended at the upper rim, and two acetoxymethyl at the lower rim which act as the arms of the tweezers and chelate the guest ion (Scheme 1). The designed sensor **L** exhibited excellent recognition capability with high selectivity and sensitivity recognition for  $\text{Ca}^{2+}$ ,  $\text{Sr}^{2+}$

and Ba<sup>2+</sup> ions over other cations. More remarkable, sensor **L** not only possessed this recognition capability but also exhibited an unexpected discrimination capability towards Ca<sup>2+</sup>, Sr<sup>2+</sup> and Ba<sup>2+</sup> ions. To the best of our knowledge, this is the first report of a chemosensor for the simultaneous recognition and discrimination Ca<sup>2+</sup>, Sr<sup>2+</sup> and Ba<sup>2+</sup>. The key element of the sensing platform is the presence of the versatile calix[4]arene scaffold with its unique 3D steric structure which is able to construct the efficient molecular tweezers.<sup>11</sup>

## EXPERIMENT SECTION

**Materials and equipment.** All solvents used were dried and distilled by standard procedures prior to use. Unless otherwise stated, all reagents used were purchased from commercial sources and were used without further purification. The solutions of the metal ions were prepared from their perchlorate salts (Aldrich and Alfa Aesar Chemical Co., Ltd.). Double distilled water was used throughout. UV-Vis absorption spectra were conducted on a UV-1800 spectrophotometer (Shimadzu) in a 1 cm quartz cell. Fluorescence spectral measurements were performed on a Cary Eclipse fluorescence spectrophotometer (Agilent Technologies) equipped with a xenon discharge lamp using a 1 cm quartz cell. <sup>1</sup>H and <sup>13</sup>C NMR spectra were recorded on a JEOL JNMELZ400S NMR spectrometer or Bruker AVANCE III 400 NMR spectrometer at room temperature using TMS as an internal standard. MALDI-TOF mass spectra were measured on a Bruker autoflex 3 system. Various pH solutions were measured using a pH meter (Orion). Cell fluorescence imaging and Zebrafish fluorescence imaging was performed using an Olympus IX73 fluorescent inverted microscope. Melting points are uncorrected. Microelectrode layers used the sputtering and lift-off process with the standard photolithography (EVG 610, Austria).

Compound **1**, **2** & **3** were prepared by following the reported procedures, and the structural identifications were verified by <sup>1</sup>H NMR spectroscopy.<sup>12</sup>

**Synthesis of sensor L.** A mixture of compound **3** (1.0 g, 1.53 mol) and 1,4-dimethylpyridinium iodide (660 mg, 2.81 mmol) in dry CHCl<sub>3</sub> (10 mL) & CH<sub>3</sub>OH (40 mL) solution was reacted at reflux under an N<sub>2</sub> atmosphere. After 10 min, 0.1 mL piperidine was added to the reaction solution. The mixture was reacted for another 3 h. After cooling to room temperature, a lot of precipitate was obtained, filtrated, and gradually washed by ether, methanol and acetone. The crude product was further purified by recrystallization from acetone to give 1.18 g of an orange solid **L** in 79 % yield. m.p. > 300 °C. <sup>1</sup>H NMR (400 MHz, DMSO-*d*<sub>6</sub>/D<sub>2</sub>O = 9/1, ppm) δ = 9.71 (s, 1H, phenol-OH), 8.65 (d, *J* = 6.7 Hz, 4H, Pyridine-H<sub>2,6</sub>), 8.05 (d, *J* = 6.6 Hz, 4H, Pyridine-H<sub>3,5</sub>), 7.79 (d, *J* = 16.4 Hz, 2H, Pyridine-CH=CH), 7.76 (s, 1H, phenol-OH), 7.62 (d, *J* = 2.8 Hz, 4H, phenol-H), 7.29 (d, *J* = 16.3 Hz, 2H, phenol-CH=CH), 7.07 (d, *J* = 7.7 Hz, 4H, Ar-H), 6.82 (t, *J* = 7.5 Hz, 2H, Ar-H), 4.81 (s, 4H, OCH<sub>2</sub>COO), 4.32 (d, *J* = 13.1 Hz, 4H, Ar-CH<sub>2</sub>-Ar), 4.17 (s, 6H, NCH<sub>3</sub>), 3.79 (s, 6H, OCH<sub>3</sub>), 3.53 (d, *J* = 13.1 Hz, 4H, Ar-CH<sub>2</sub>-Ar). <sup>13</sup>C NMR (101 MHz, DMSO-*d*<sub>6</sub>) δ = 30.77, 31.05, 47.14, 52.58, 72.68, 72.72, 120.32, 123.20, 126.02, 126.06, 126.98, 128.93, 128.98, 129.01, 129.65, 129.70, 129.76, 129.79, 131.41, 133.21, 133.42, 133.44, 141.60, 145.25, 152.76, 153.44, 155.74, 155.81, 159.07, 169.81, 169.83 and 191.38 ppm. HRMS(ESI): *m/z*

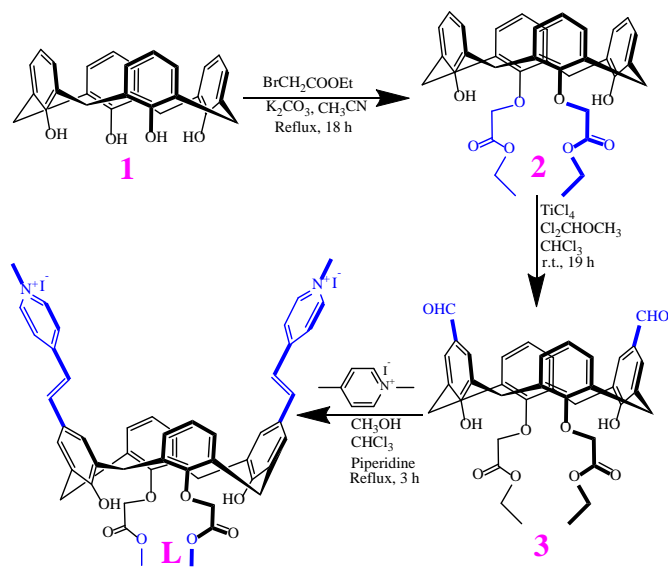
Calcd. for C<sub>50</sub>H<sub>48</sub>N<sub>2</sub>O<sub>8</sub>I<sub>2</sub>-2I<sup>-</sup>: 402.1700 [**L**-2I]<sup>2+</sup>, found 402.1718 (Fig. S1-S3).

**Spectral measurements.** The recognition properties of sensor **L** toward various metal ions (Li<sup>+</sup>, Na<sup>+</sup>, K<sup>+</sup>, Mg<sup>2+</sup>, Ca<sup>2+</sup>, Ba<sup>2+</sup>, Sr<sup>2+</sup>, Cr<sup>3+</sup>, Al<sup>3+</sup>, Co<sup>2+</sup>, Ni<sup>2+</sup>, Cu<sup>2+</sup>, Pb<sup>2+</sup>, Cd<sup>2+</sup>, Ag<sup>+</sup>, Hg<sup>2+</sup>, Fe<sup>3+</sup>, Mn<sup>2+</sup>, Zn<sup>2+</sup>) were investigated by UV-vis and fluorescence spectroscopy. To a 10 mL volumetric flask containing different amounts of ions, the appropriate amounts of the solution of sensor **L** were added using a micropipette. For Ca<sup>2+</sup>, Sr<sup>2+</sup> and Ba<sup>2+</sup>, the system was then diluted with DMF/H<sub>2</sub>O (9/1, v/v, pH = 8.5) mixed solvent to 10 mL, and then the fluorescence sensing of the ions was conducted. The fluorescence spectra were measured after addition of the ions at room temperature and when the equilibrium was reached. Fluorescence measurements were carried out with an excitation and emission slit width of 10 nm.

**Cell culture and fluorescence imaging.** HeLa cells were grown using a Roswell Park Memorial Institute (RPMI) 1640 supplemented with 10% fetal bovine serum, 1 IU/mL penicillin and 1 IU/mL streptomycin at 37 °C and 5% CO<sub>2</sub>. One day prior to imaging, the cells were seeded in 96-well flat-bottomed plates. The next day, the cells were incubated with 25 μM of probe **L** for 90 min. at 37 °C in PBS solution (without RPMI-1640 medium). The cells were rinsed with PBS solution three times to remove the remaining probe, fluorescent images of intracellular probe were collected with an inverted fluorescence microscope (Olympus IX73) with Nikon color camera. After that, the treated cells were further incubating with Ca<sup>2+</sup>, Sr<sup>2+</sup> or Ba<sup>2+</sup> (200 μM, culture medium/H<sub>2</sub>O = 9/1, v/v) for another 90 min., respectively. The cells were rinsed with PBS solution three times to remove the remaining cations, then fluorescent images of intracellular Ca<sup>2+</sup>, Sr<sup>2+</sup> or Ba<sup>2+</sup> were collected again with an inverted fluorescence microscope (Olympus IX73) with NIKON color camera.

**Zebrafish imaging.** All animal procedures were performed in accordance with the Guidelines for Care and Use of Laboratory Animals of Shenzhen Institutes of Advanced Technology, Chinese Academy of Sciences and approved by the Animal Ethics Committee of Shenzhen Institutes of Advanced Technology, Chinese Academy of Sciences (IACUC NO: SIAI-IACUC-190111-YGS-ZJL-A0556). Zebrafish were maintained in an E3 embryo medium with 1-Phenyl-2-Thiourea (PTU, 0.0045%). In fluorescence imaging experiments, three-day-old zebrafish were incubated with the sensor **L** (3 μL, 1 mM, DMSO) in 1 mL of double distilled water for 30 min. at room temperature. After washing three times with double distilled water to remove the remaining probes, the Zebrafish were anesthetized by MS-222 and visualized using an inverted fluorescence microscope (Olympus IX73) with 4× objective lens.

**Determination of cytotoxicity by CCK-8 assay.** The relative cell growth was evaluated with the Cell Counting Kit-8 (CCK-8, MedChem Express) in accordance with the manufacturer's instruction. Briefly, HeLa cell were seeded into a 96-well plate at a concentration of 4×10<sup>4</sup> cells per well in triplicate for 24 h of consecutive culture. The cells were treated with different concentrations of probe **L** (0, 10, 25, 50 and 100 μM) for about 24 h. in a humidified incubator at 37 °C, 5% CO<sub>2</sub>. 10μL CCK-8 reagent was added to each well of the plate, followed by incubation at 37 °C for 1.5 h. The OD450 was measured at 450 nm with a microplate reader.



**Scheme 1.** The synthetic route to sensor **L**.

## RESULT AND DISCUSSION

**Synthesis.** Compound **1**, **2** & **3** were prepared as reported in the literature, and the structural identification verified by  $^1\text{H}$  NMR spectroscopy.<sup>12</sup> The target compound (**L**) was synthesized via the Knoevenagel reaction (Scheme 1). The two new doublets at  $\delta$  7.79 ppm (2H) &  $\delta$  7.29 ppm (2H) in the proton NMR spectrum correspond to the ethylenic linkage (CH=CH), indicating that the reaction was successful (Fig. S1). On the other hand, as piperidine is a strong organic base, the ethyl group of compound **3** should normally be hydrolyzed to an acid during this reaction. However, surprisingly, when we further analyzed the  $^1\text{H}$  NMR spectrum, the ethyl protons of compound **3** were unexpectedly replaced by a singlet at  $\delta$  3.79 ppm (6H), which when combined with the corresponding carbon signal at  $\delta$  52.58 ppm in the  $^{13}\text{C}$  NMR spectrum (Fig. S2), was consistent with the presence of a new methoxy group (OCH<sub>3</sub>). The new methoxy group can be attributed to an ester exchange reaction.<sup>13</sup> The structure of sensor **L** was also verified by  $^1\text{H}/^{13}\text{C}$  NMR and ESI-HRMS (Fig. S3,  $m/z$ : [**L**-2]<sup>2+</sup> Calcd. for C<sub>50</sub>H<sub>48</sub>N<sub>2</sub>O<sub>8</sub> 402.1700, found 402.1718).

Interestingly, the unexpected introduction of the acetoxymethyl groups in sensor **L** resulted in an enhancement of cell permeability which had proposed by Tsien in 1981<sup>14</sup> and confirmed later by others.<sup>15</sup> Moreover, the introduction of the methylpyridinium iodide motifs not only act as a fluorophore but also greatly increased the water solubility. Indeed, sensor **L** can be dissolved (more than 90%) in water/organic (DMSO, DMF, THF & CH<sub>3</sub>CN) mixtures. Consequently, sensor **L** is a good candidate for *in vivo* studies, such as cell imaging and zebrafish imaging.

**The recognition capability of sensor L towards cations.** The design of compound **L** means that it can serve as a chemosensor. Consequently, the recognition properties of sensor **L** were explored. After evaluating the effect of the water content and pH (Fig. S4), we selected the DMF/H<sub>2</sub>O (9/1, pH = 8.5) mixture for these studies. As shown in figure 1a, probe **L** exhibited a pale orange color with an intense absorption band (wavelength 405 nm). Following addition of 20 equiv. of Ca<sup>2+</sup>, Sr<sup>2+</sup> or Ba<sup>2+</sup> cations, a dramatic red shift can

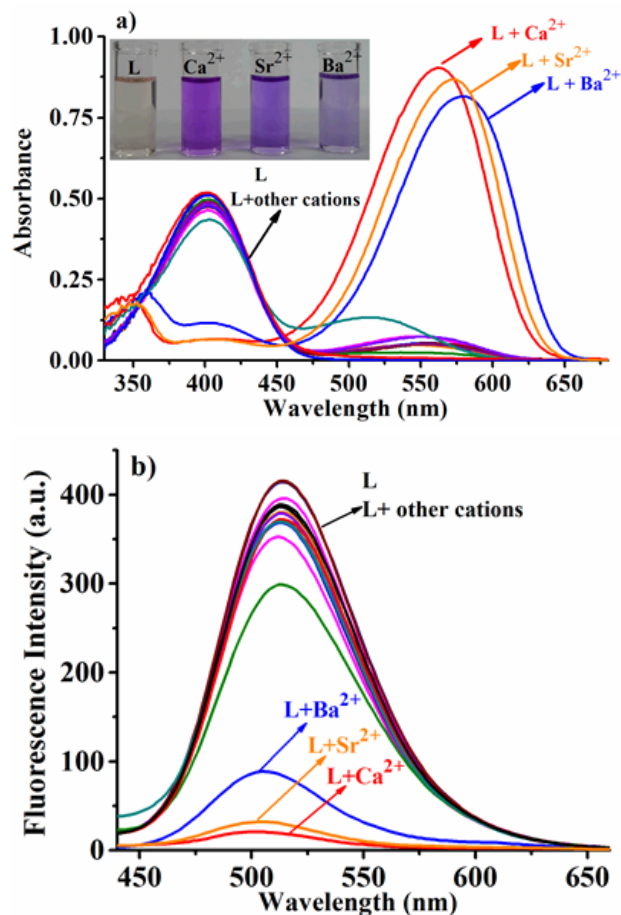


**Figure 1.** Absorption spectra (a) or fluorescence spectra (b,  $\lambda_{\text{ex}} = 405$  nm) of sensor **L** (10  $\mu\text{M}$ , DMF/H<sub>2</sub>O = 9/1, pH = 8.5) with or without 20 equiv. of the various anions. (inset) The color changes of the sensor **L** with or without Ca<sup>2+</sup>, Sr<sup>2+</sup> or Ba<sup>2+</sup> under sunlight. Other tested ions include Li<sup>+</sup>, Na<sup>+</sup>, K<sup>+</sup>, Ag<sup>+</sup>, Mg<sup>2+</sup>, Hg<sup>2+</sup>, Zn<sup>2+</sup>, Cd<sup>2+</sup>, Ni<sup>2+</sup>, Co<sup>2+</sup>, Cu<sup>2+</sup>, Pb<sup>2+</sup>, Fe<sup>3+</sup>, Al<sup>3+</sup> and Cr<sup>3+</sup>.

be observed at 560 nm for Ca<sup>2+</sup>, 570 nm for Sr<sup>2+</sup> and 580 nm for Ba<sup>2+</sup>, respectively. Interestingly, we find that the red shift is in the sequence of Ca<sup>2+</sup> (155 nm) < Sr<sup>2+</sup> (165 nm) < Ba<sup>2+</sup> (175 nm) which matches their radius sequence [Ca<sup>2+</sup> (1.8 Å) < Sr<sup>2+</sup> (2.0 Å) < Ba<sup>2+</sup> (2.15 Å)].<sup>16</sup> From this, it can be implied that sensor **L** has the ability to distinguish between the group IIA elements based on their atomic radii. There were no significant changes upon the addition of other cations, which indicated the high selectivity of sensor **L** toward these three alkaline earth metal cations. The dramatic red shift resulted in an obvious colour change which enable us to directly monitor Ca<sup>2+</sup>, Sr<sup>2+</sup> or Ba<sup>2+</sup> by the naked eye (Fig. 1a, inset). Similar selectivity has been observed in the fluorescence spectra; only the presence of Ca<sup>2+</sup>, Sr<sup>2+</sup> or Ba<sup>2+</sup> resulted in a significant decrease in fluorescence which indicated high selectivity of sensor **L** towards the cation Ca<sup>2+</sup>, Sr<sup>2+</sup> and Ba<sup>2+</sup> (Fig. 1b).

In further investigate the recognition processes, UV-vis and fluorescence (FL) titration experiments were conducted. On increasing the concentration of Ca<sup>2+</sup>, the absorption at 405 nm gradually diminished, whilst the absorption at 560 nm significantly increased with an isobestic point at 455 nm (Fig. 2a). Equilibrium was reached upon addition of one equiv. Ca<sup>2+</sup>, consistent with a 1:1 complex for the sensor **L** and Ca<sup>2+</sup>

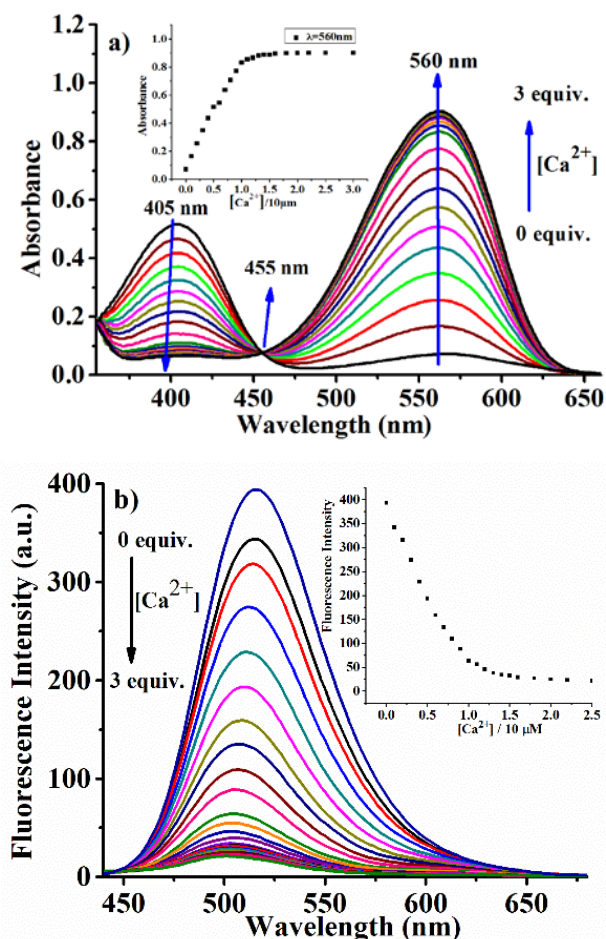


**Figure 2.** Absorption spectra (a) or fluorescence spectra (b,  $\lambda_{ex} = 405$  nm) changes of sensor **L** ( $10 \mu\text{M}$ , DMF/ $\text{H}_2\text{O} = 9/1$ ,  $\text{pH} = 8.5$ ) solution upon addition of  $\text{Ca}^{2+}$  (0 ~ 3 equiv.). Inset: the plot of absorption or fluorescence intensity of sensor **L** as a function of  $\text{Ca}^{2+}$  concentration.

(Fig. 2a inset). The observed ratiometric absorption changes revealed that sensor **L** can behave as a ratiometric sensor for  $\text{Ca}^{2+}$ . It is recognized that ratiometric responsive probes are superior to other type of probe given their built-in correction for environmental effects and self-correcting capability.<sup>17</sup> On the other hand, the fluorescence titration experiments revealed a fluorescence quenching phenomenon upon increasing the amount of  $\text{Ca}^{2+}$  (Fig. 2b). A 1:1 complex ratio can be found with the complex equilibrium in the presence of one equiv. of  $\text{Ca}^{2+}$  (Fig. 2b, inset). The 1:1 complex stoichiometry for sensor **L** towards  $\text{Ca}^{2+}$  was further confirmed by a Job plot's analysis (Fig. S5a). Similar features can be observed upon the addition of  $\text{Sr}^{2+}$  (Fig. S6) and  $\text{Ba}^{2+}$  (Fig. S7) in both UV-vis and FL titration experiments, albeit with slightly different values. These three complexes ( $\text{L}\cdot\text{Ca}^{2+}$ ,  $\text{L}\cdot\text{Sr}^{2+}$  and  $\text{L}\cdot\text{Ba}^{2+}$ ) exhibited a 1:1 complex stoichiometry (Fig.2 & Fig. S6~7 inset, Fig. S5).

The potential application of sensor **L** ( $10 \mu\text{M}$ ) as a selective sensor for  $\text{Ca}^{2+}$ ,  $\text{Sr}^{2+}$  or  $\text{Ba}^{2+}$  ions has been investigated by using 'co-existing' experiments. For example, in the presence of the  $\text{L}\cdot\text{Ca}^{2+}$  complex solution, when mixed with 20 equiv. of any other potentially interfering cations  $\text{Li}^+$ ,  $\text{Na}^+$ ,  $\text{K}^+$ ,  $\text{Ag}^+$ ,  $\text{Mg}^{2+}$ ,  $\text{Sr}^{2+}$ ,  $\text{Ba}^{2+}$ ,  $\text{Hg}^{2+}$ ,  $\text{Zn}^{2+}$ ,  $\text{Cd}^{2+}$ ,  $\text{Ni}^{2+}$ ,  $\text{Co}^{2+}$ ,  $\text{Cu}^{2+}$ ,  $\text{Pb}^{2+}$ ,  $\text{Fe}^{3+}$ ,  $\text{Al}^{3+}$  and  $\text{Cr}^{3+}$ , no significant interference was observed in

either the UV-vis (Fig. S8a) or fluorescent spectra (Fig. S9a) except for  $\text{Sr}^{2+}$  and  $\text{Ca}^{2+}$ . The same features have been observed in the case of  $\text{L}\cdot\text{Sr}^{2+}$  and  $\text{L}\cdot\text{Ba}^{2+}$  (Fig. S8b~c & Fig. S9b~c). Moreover, we can further discriminate between these three cations based on their differing max absorption peak (560 nm for  $\text{Ca}^{2+}$ , 570 nm for  $\text{Sr}^{2+}$  and 580 nm for  $\text{Ba}^{2+}$ ) in the UV-vis spectra (Fig. 1a). In other words, the presence of these three cations was not detrimental to the detection of each of them individually. Consequently, all of this data clearly suggested that sensor **L** was capable of acting as a highly selective sensor for  $\text{Ca}^{2+}$ ,  $\text{Sr}^{2+}$  and  $\text{Ba}^{2+}$  in the presence of the above tested cations in practical applications.

For a good chemosensor, as well as the high selectivity, high sensitivity is also very important. The higher sensitivity, the lower the limit of detection (LOD). The limit of detection of sensor **L** towards  $\text{Ca}^{2+}$ ,  $\text{Sr}^{2+}$  and  $\text{Ba}^{2+}$  were calculated to be in the region of  $10^{-7}$  to  $10^{-8}$  M according to the formula:  $\text{LOD} = 3\sigma/\text{slope}$  (Fig. S10 ~ S11 & Table 1). These lower LODs indicated that sensor **L** is very sensitive for the detection of the  $\text{Ca}^{2+}$ ,  $\text{Sr}^{2+}$  and  $\text{Ba}^{2+}$  cations. Another important analysis parameter for a chemosensor is the association constant ( $K_a$ ). The  $K_a$  for  $\text{L}\cdot\text{Ca}^{2+}$ ,  $\text{L}\cdot\text{Sr}^{2+}$  and  $\text{L}\cdot\text{Ba}^{2+}$  complexes were calculated by nonlinear fitting according to the method of Thodarson (Fig. S12 ~ S13, Table 1).<sup>18</sup> No matter whether calculating from the fluorescence data or the UV-vis data, both

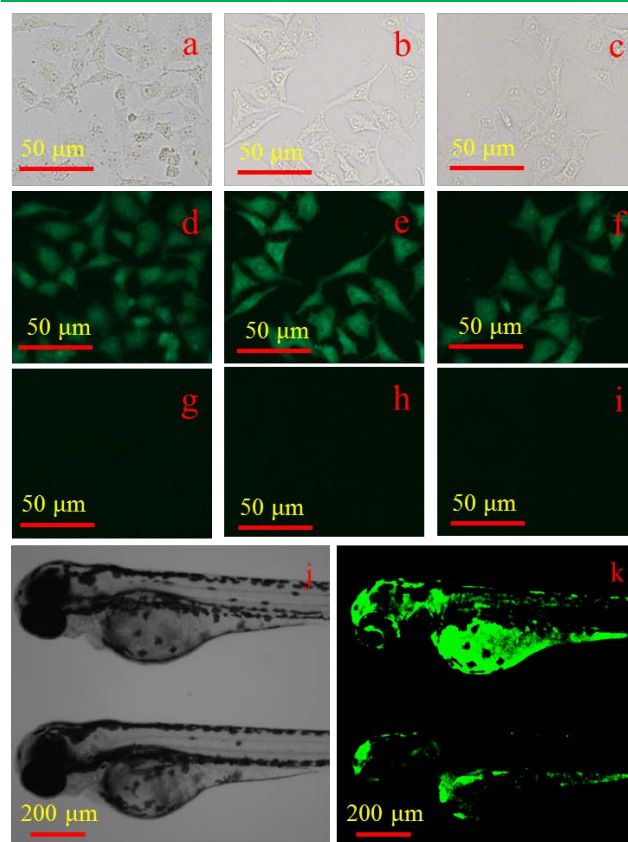


**Figure 3.** Fluorescence microscopy images of HeLa cells treated with  $25 \mu\text{M}$  sensor **L** (a ~ c, Bright field) and (d ~ f, Green channel); (g ~ i) HeLa cells pre-treated with sensor **L**, then treated with  $\text{Ca}^{2+}$ ,  $\text{Sr}^{2+}$  or  $\text{Ba}^{2+}$  ion, respectively. (j) Zebrafish treated with (the up Zebrafish)/ without (the bottom Zebrafish)  $3 \mu\text{M}$  sensor **L** in the bright field; (k) Zebrafish treated with (the up Zebrafish)/ without (the bottom Zebrafish)  $3 \mu\text{M}$  sensor **L** under the green channel.

**Table 1. Analysis parameters for sensor L and detection of Ca<sup>2+</sup>, Sr<sup>2+</sup> and Ba<sup>2+</sup>.**

Cations	Method	The linear range of the calibration curve (M)	Correlation coefficient	Limits of detection (M)	Association constants $K_a$ (M <sup>-1</sup> )
Ca <sup>2+</sup>	UV-vis (560 nm)	$1.0 \times 10^6 \sim 1.0 \times 10^5$	0.9916	$1.33 \times 10^{-7}$	$K_a = 8.1451 \times 10^6$
	FL	$1.0 \times 10^6 \sim 1.0 \times 10^5$	0.9843	$7.51 \times 10^{-8}$	$K_a = 5.1746 \times 10^6$
Sr <sup>2+</sup>	UV-vis (570 nm)	$1.0 \times 10^6 \sim 1.0 \times 10^5$	0.9832	$1.53 \times 10^{-7}$	$K_a = 2.0301 \times 10^6$
	FL	$1.0 \times 10^6 \sim 1.0 \times 10^5$	0.9812	$9.08 \times 10^{-8}$	$K_a = 1.1355 \times 10^6$
Ba <sup>2+</sup>	UV-vis (580 nm)	$1.0 \times 10^6 \sim 1.0 \times 10^5$	0.9699	$2.23 \times 10^{-7}$	$K_a = 1.0501 \times 10^6$
	FL	$1.0 \times 10^6 \sim 1.0 \times 10^5$	0.9659	$1.44 \times 10^{-7}$	$K_a = 1.3258 \times 10^6$

methods gave a high  $K_a$  value (up to the order of  $10^6$  M<sup>-1</sup>) which revealed that the **L**•Ca<sup>2+</sup>, **L**•Sr<sup>2+</sup> and **L**•Ba<sup>2+</sup> complexes were very stable. Under the optimal conditions, the detection analysis parameters for sensor **L** toward Ca<sup>2+</sup>, Sr<sup>2+</sup> and Ba<sup>2+</sup> are summarized in table 1. This data revealed that sensor **L** is a prime candidate for use in the detection of Ca<sup>2+</sup>, Sr<sup>2+</sup> and Ba<sup>2+</sup> cations.

**Fluorescence sensing and imaging (*in vivo*) of sensor L in living cell, zebrafish.** Given sensor **L** is highly water solubility and the acetoxymethyl group affords good cell permeability, the bioimaging application of sensor **L** in Hela cell has been assessed. Cellular viability assay under various concentrations (0  $\mu$ M, 10  $\mu$ M, 25  $\mu$ M, 50  $\mu$ M, 100  $\mu$ M and 200  $\mu$ M) of sensor **L** have been performed (Fig. S19) which revealed low toxicity for sensor **L**. The low cytotoxicity was further confirmed by using CCK-8 (Cell Counting Kit-8) assays. This was performed by directly determining the effect of sensor **L** on the cellular viability of Hela cell. The Hela cells were either treated with various concentrations of sensor **L** (10  $\mu$ M, 25  $\mu$ M, 50  $\mu$ M and 100  $\mu$ M) or as a control left untreated. The results revealed that sensor **L** at the concentrations 10, 25, 50 and 100  $\mu$ M had little significant effect ( $P < 0.01$ ) on cell viability over a 24 h period (Fig. S20). Considering the quality of cell imaging and the possible cell toxicity, 25  $\mu$ M sensor **L** has been employed throughout the cell imaging experiment. Bright-field measurements confirmed that the Hela cells, following treatment with sensor **L**, were viable throughout the imaging experiments (Fig. 3a ~ c). When the Hela cells were incubated with 25  $\mu$ M of sensor **L** for 90 min., a significant green fluorescence from the intracellular area (Fig. 3d ~ f) could be observed which demonstrates that sensor **L** is permeable to Hela cells. We should point out that, according to our fluorescence spectral results (Fig. 1b & Fig. 2b), the presence of Ca<sup>2+</sup> will induce the fluorescence quenching of sensor **L**. Consequently, using RPMI-1640 culture medium containing some Ca<sup>2+</sup> would greatly disturb the cell imaging experiment. Hence, during the incubation with sensor **L** process, we used PBS solution instead with RPMI-1640 culture medium. Otherwise, only weak fluorescence in the cell imaging is observed. As expected, when we directly added plenty of alkaline earth metal cations (200  $\mu$ M, Ca<sup>2+</sup>, Sr<sup>2+</sup> & Ba<sup>2+</sup>), the corresponding fluorescence was completely quenched (Fig. 3g ~ 3i). This can be attributed to the Ca<sup>2+</sup>, Sr<sup>2+</sup> and Ba<sup>2+</sup> cations which permeated to the cells, and then can be complexed by the intracellular sensor **L** resulting in the observed fluorescence quenching.

***In vivo* imaging.** The excellent cell penetrability of sensor **L** encouraged us to explore its potential for applications *in vivo*.

Zebrafish is a popular vertebrate model organism which has been extensively applied for fluorescence imaging given its favorable characteristics which include ca. 87% homologous genes with humans, small size, and embryos transparency.<sup>19</sup> Thus, 3-day-old zebrafish in E3 embryo media was employed as the *in vivo* model to explore the properties of sensor **L**. Due to the Zebrafish itself having a certain autofluorescence, in order to eliminate the background effect, we selected a pair of Zebrafish (treated and untreated with 3  $\mu$ M sensor **L**<sup>20</sup>) to do the fluorescence imaging at the same time. Under these

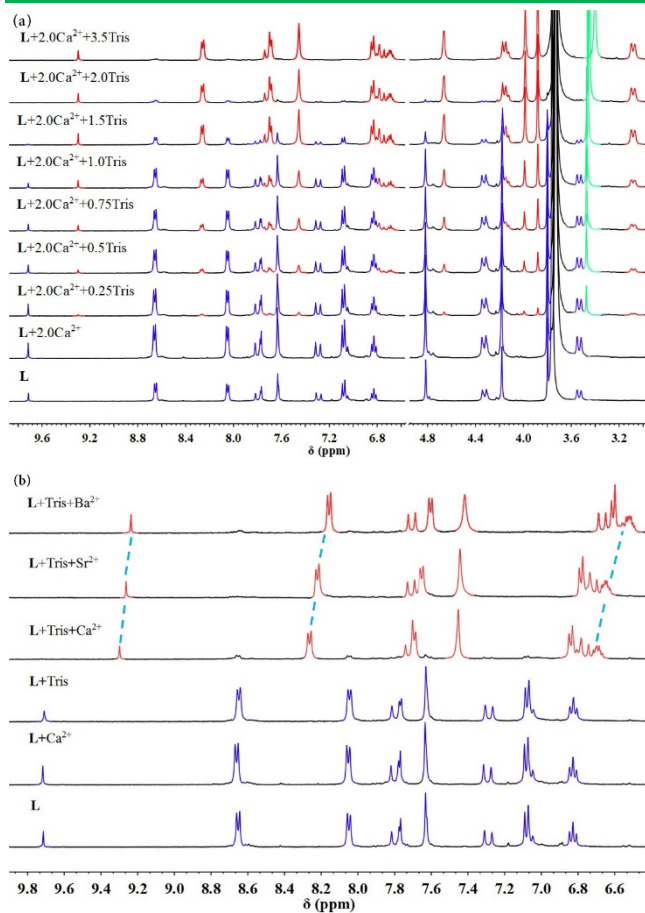


**Figure 4.** (a) Partial <sup>1</sup>H NMR spectra of sensor **L** with 2.0 equiv. Ca<sup>2+</sup> and increasing concentrations (0 ~ 3.5 equiv.) of Tris in DMSO-*d*<sub>6</sub>/D<sub>2</sub>O = 9/1 at 298K. (b) Partial <sup>1</sup>H NMR spectra of sensor **L**, **L** with plenty of Ca<sup>2+</sup>, **L** with plenty of Tris, **L** with plenty of Tris and Ca<sup>2+</sup> or Sr<sup>2+</sup> or Ba<sup>2+</sup>. Blue peaks assign to sensor **L**; Red peaks assign to sensor **L** after complex; Green peaks assign to Tris.

comparable conditions, it is clearly observed that the presence of sensor **L** induced an increase in the acute fluorescence signal (Fig. 3j ~ k). In other words, sensor **L** also can readily be taken up by Zebrafish which makes it a potential candidate as a fluorescence imaging indicator in zebrafish. All of these results indicated that sensor **L** can be utilized in the imaging of living cells and Zebrafish *in vivo*.

**The recognition mechanism of sensor **L** towards  $\text{Ca}^{2+}$ ,  $\text{Sr}^{2+}$  and  $\text{Ba}^{2+}$  cations.** To more fully understand the recognition mechanism of sensor **L** toward  $\text{Ca}^{2+}$ ,  $\text{Sr}^{2+}$  and  $\text{Ba}^{2+}$ ,  $^1\text{H}$  NMR spectroscopic titration experiments have been conducted using their perchlorate salts. Disappointingly, when we directly increased the concentration of  $\text{Ca}^{2+}$  in the solution of sensor **L**, no significant chemical shifts could be observed (Fig. S14). Considering the FL and UV-vis experiments are conducted under weakly basic conditions (Tris-HCl buffer, pH = 8.5), we added some Tris buffer solution to the above NMR tube (containing 2.0 equiv.  $\text{Ca}^{2+}$  solution) to adjust the solution pH. Surprisingly, upon increasing the concentration of Tris, all of the proton signals (blue peaks) of sensor **L** were gradually replaced by a new group of up-field signals (red peaks), except for the  $\text{OCH}_3$  (Fig. 4a) resonance. Conversion was near complete after the addition of two equiv. of Tris (1:2 stoichiometry), which strongly suggested that the Tris make a contribution to the recognition complex. However, on increasing the Tris concentration without the assistance of  $\text{Ca}^{2+}$ , no proton signal changes can be observed (Fig. S15). This revealed that the recognition process must be a cooperation between the  $\text{Ca}^{2+}$  and Tris. Further, when we changed the addition sequence, *i.e.* we first added plenty of Tris, and then gradually increased the concentration of  $\text{Ca}^{2+}$ , the same changes can be observed (Fig. S16). This indicated that the proton signal changes are not affected by the addition sequence, and complete conversion to the corresponding new signals was observed after addition of one equiv. of  $\text{Ca}^{2+}$ . This 1:1 stoichiometry is agreed with the UV-vis and FL titration results (Fig. 2 & Fig. S5).

Similar results were observed in the case of  $\text{Sr}^{2+}$  and  $\text{Ba}^{2+}$  (Fig. S17~S18). It is worth pointing out that the unique phenomenon here is that all the proton signal of sensor **L** completely convert to a new set of signals after complexation, and this is not the same as the traditional complexation mechanism. Usually, for traditional  $^1\text{H}$  NMR titration experiments on complexation studies, large chemical shift changes are only observed near the binding site and not for all of the protons.<sup>17a,21</sup> However, our observations is that all of the original proton signals are directly replaced by a set of new signals with the new peaks appearing up-field (Fig. 4, S16~S18). Hence, we speculate that the whole molecular framework of sensor **L** is plunged into a higher shielding field induced by  $\text{Ca}^{2+}/\text{Sr}^{2+}/\text{Ba}^{2+}$  and Tris. Given the presence of ester group ( $\text{OCH}_2\text{COOCH}_3$ ) in sensor **L**, according to Tsien's research<sup>8,14</sup> and recent reviews<sup>7e,7f</sup> for the alkaline earth metal ion chemosensors, the best binding site for  $\text{Ca}^{2+}/\text{Sr}^{2+}/\text{Ba}^{2+}$  in sensor **L** is the  $\text{OCH}_2\text{COOCH}_3$  moiety. Combining the stoichiometry ratio for sensor **L**: alkaline earth metal ion: Tris is 1:1:2. Consequently, a plausible binding model for sensor **L** with  $\text{Ca}^{2+}/\text{Sr}^{2+}/\text{Ba}^{2+}$  and Tris have been proposed herein, as shown in Fig. 5.

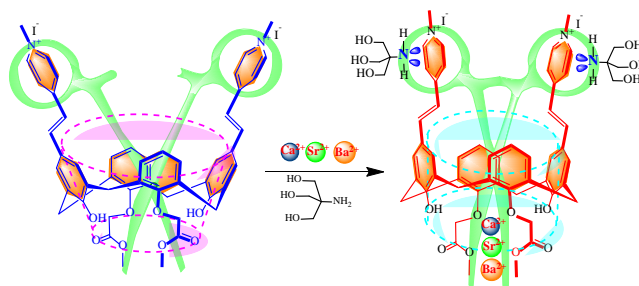


**Figure 5.** A plausible binding model of the sensor **L** with  $\text{Ca}^{2+}/\text{Sr}^{2+}/\text{Ba}^{2+}$  ion and Tris.

The free sensor **L** exhibits a classic cone conformation with an open molecular tweezer-like structure (Fig. 5 Left). After addition of  $\text{Ca}^{2+}$  or  $\text{Sr}^{2+}$  or  $\text{Ba}^{2+}$  and the Tris solution, the alkaline earth metal ion was chelated by the two ester groups at the lower rim which forced the adjacent benzene ring to be face-to-face and thereby formed a stronger  $\pi$ - $\pi$  interaction to increase the shielding effect. The degree of shielding effect (chemical shift changing value,  $\Delta\delta$ ) followed the radius sequence of  $\text{Ca}^{2+} < \text{Sr}^{2+} < \text{Ba}^{2+}$  (Fig. 4b) which is exactly same as observed for the UV-vis red-shift results (Fig. 1a). This may be attributed to the position of the added ions which then dictates the degree of  $\pi$ - $\pi$  interaction. On the other hand, the proton signal for the Tris was shifted down-field (Fig. S16~S18, Green peak), which may be attributed to the lone pair- $\pi$  interactions,<sup>22</sup> the electron cloud of the nitrogen (lone pair) atom of the  $\text{NH}_2$  group which was attracted by the electron deficiency of the methylpyridinium ring (electron-deficient  $\pi$ -systems) and resulted in a deshielding effect for the  $\text{CH}_2$  group of Tris (Fig. 5). The two Tris molecules pushed the tweezers arms (the two methylpyridinium group) toward the center of the calix[4]arene scaffold and formed another strong  $\pi$ - $\pi$  interaction to increase the shielding effect. Finally, under the cooperation of  $\text{Ca}^{2+}$  or  $\text{Sr}^{2+}$  or  $\text{Ba}^{2+}$  with Tris, the open molecular tweezers were closed, and the original cone conformation of sensor **L** was converted to a pillar-like conformation (Fig.5 Right). All of the aromatic moieties are then face-to-face and form a large shielding field which resulted in all of the protons associated with **L** appearing up-field.

## CONCLUSIONS

In conclusion, a molecular tweezer based on the calix[4]arene chemosensor **L** has been designed. Sensor **L** exhibited high selectivity and sensitivity towards the alkaline earth metal ions  $\text{Ca}^{2+}/\text{Sr}^{2+}/\text{Ba}^{2+}$ . Furthermore, sensor **L** possesses the capability to distinguish between  $\text{Ca}^{2+}$ ,  $\text{Sr}^{2+}$ ,  $\text{Ba}^{2+}$  according to their different max absorption wavelength (560 nm for  $\text{Ca}^{2+}$ , 570 nm for  $\text{Sr}^{2+}$  and 580 nm for  $\text{Ba}^{2+}$ ), or according to their different color by the naked eye. The successful fluorescence sensing and imaging of sensor **L** in living cells indicated that sensor **L** possesses good cell penetrability, and it can be utilized to sense and image in Zebrafish *in vivo*. Significantly, a rare synergistic effect recognition mechanism have been identified here for the first time. The whole molecule **L** experiences a high shielding field via the cooperation of the Tris and the alkaline earth metal ion with the result that all of the proton signals of sensor **L** appeared up-field.

## ASSOCIATED CONTENT

### Supporting Information.

Detailed characterization, spectra and  $^1\text{H}$  NMR titration data (PDF). This material is available free of charge via the Internet at <http://pubs.acs.org>.

## AUTHOR INFORMATION

### Corresponding Authors

- \* E-mail: [jl.zhao@siat.ac.cn](mailto:jl.zhao@siat.ac.cn) (J.-L. Zhao);
- \* E-mail: [zengxi1962@163.com](mailto:zengxi1962@163.com) (X. Zeng);
- \* E-mail: [zw.jin@siat.ac.cn](mailto:zw.jin@siat.ac.cn) (Z. Jin);

### Notes

The authors declare no competing financial interest.

## ACKNOWLEDGMENT

This work was supported by the Basic Research Program of Shenzhen (JCYJ20170818161714678, JCYJ20170413153034718), the “Chun-Hui” Fund of Chinese Ministry of Education (Z2016008) and the SIAT Innovation Program for Excellent Young Researchers (2017014). CR thanks the EPSRC for an Overseas Travel grant (EP/R023816/1).

## REFERENCES

- (1) Nordin, B. E. C. *Calcium in Human Biology*; Springer-Verlag: London, 1988.
- (2) (a) Clapham, D. E. Calcium signaling. *Cell* **2007**, *131*, 1047–1058; (b) Kuchibhotla, K. V.; Lattarulo, C. R.; Hyman, B. T.; Bacskaï, B. J. Synchronous hyperactivity and intercellular calcium waves in astrocytes in alzheimer mice. *Science* **2009**, *323*, 1211–1215.
- (3) (a) Salido, A.; Jones, B. The use of aluminum and potassium as modifiers to improve the determination of strontium by tungsten coil atomic emission spectrometry. *Anal. Lett.* **2011**, *44*, 2760–2767; (b) Acton, J. M.; Rogers, M. B.; Zimmerman, P. D. Beyond the dirty bomb: Re-thinking radiological terror. *Survival* **2007**, 151–168.
- (4) Kelemen, J.; Szakács, O.; Lásztity, A. Determination of barium by atomic absorption spectrometry with electrothermal atomisation. Part I. Study of the volatilisation and atomisation of solid barium phosphate, silicate, molybdate, vanadate and molybdovanadate compounds. *J. Anal. At. Spectrom.* **1990**, *5*, 377–384.
- (5) Patnaik, P. *Handbook of inorganic chemicals*, New York: McGraw-Hill, 2003, 77–79
- (6) (a) Carter, K. P.; Young, A. M.; Palmer, A. E. Fluorescent sensors for measuring metal ions in living systems. *Chem. Rev.* **2014**, *114*, 4564–4601; (b) Wu, J.; Kwon, B.; Liu, W.; Anslyn, E. V.; Wang, P.; Kim, J. S. Chromogenic/fluorogenic ensemble chemosensing systems. *Chem. Rev.* **2015**, *115*, 7893–7943; (c) Ashton, T. D.; Jolliffe, K. A.; Pfeffer, F. M. Luminescent probes for the bioimaging of small anionic species in vitro and in vivo. *Chem. Soc. Rev.* **2015**, *44*, 4547–4595; (d) Jung, H. S.; Verwilt, P.; Kim, W. Y.; Kim, J. S. Fluorescent and colorimetric sensors for the detection of humidity or water content. *Chem. Soc. Rev.* **2016**, *45*, 1242–1256; (e) Wu, D.; Sedgwick, A. C.; Gunnlaugsson, T.; Akkaya, E. U.; Yoon, J.; James, T. D. Fluorescent chemosensors: the past, present and future. *Chem. Soc. Rev.* **2017**, *46*, 7105–7123.
- (7) (a) Liu, Z.; Jing, X.; Zhang, S.; Tian, Y. A copper nanocluster-based fluorescent probe for real-time imaging and ratiometric biosensing of calcium ions in neurons. *Anal. Chem.* **2019**, *91*, 2488–2497; (b) Zhang, H.; Yin, C.; Liu, T.; Zhang, Y.; Huo, F. “Turn-on” fluorescent probe detection of  $\text{Ca}^{2+}$  ions and applications to bioimaging. *Spectrochim. Acta. A* **2017**, *180*, 211–216; (c) Kim, H. J.; Lim, C. S.; Lee, H. W.; Lee, H. S.; Um, Y. J.; Kumar, H.; Han, I.; Kim, H. M. A ratiometric two-photon probe for  $\text{Ca}^{2+}$  in live tissues and its application to spinal cord injury model. *Biomaterials* **2017**, *141*, 251–259; (d) Zhou, W.; Zhang, Y.; Ding, J.; Liu, J. In vitro selection in serum: RNA-cleaving DNazymes for measuring  $\text{Ca}^{2+}$  and  $\text{Mg}^{2+}$ . *ACS. Sensors* **2016**, *1*, 600–606; (e) Yin, J.; Hu, Y.; Yoon, J. Fluorescent probes and bioimaging: alkali metals, alkaline earth metals and pH. *J. Chem. Soc. Rev.* **2015**, *44*, 4619–4644; (f) Hamilton, G. R.; Sahoo, S. K.; Kamila, S.; Singh, N.; Kaur, N.; Hyland, B. W.; Callan, J. F. Optical probes for the detection of protons, and alkali and alkaline earth metal cations. *Chem. Soc. Rev.* **2015**, *44*, 4415–4432.
- (8) Grynkiewicz, G.; Poenie, M.; Tsien, R. Y. A new generation of  $\text{Ca}^{2+}$  indicators with greatly improved fluorescence properties. *Biol. Chem.* **1985**, *260*, 3440–3450.
- (9) (a) Zhang, Q.; Duan, K. Fluorescence chemosensor containing 4-methyl-7-coumarinyloxy, acetylhydrazono and N-phenylaza-15-crown-5 moieties for  $\text{K}^{+}$  and  $\text{Ba}^{2+}$  ions. *Heterocycl. Commun.* **2018**, *24*, 141–145; (b) Patel, K.; Bhamore, J. R.; Park, T. J.; Kailasa, S. K. Selective and sensitive colorimetric recognition of  $\text{Ba}^{2+}$  ion using guanine-functionalized silver nanoparticles. *ChemistrySelect* **2018**, *3*, 10182–10187; (c) Lin, F.; Hu, Y.; Wu, T.; Zhou, X.; Shao, Y. Aggregation/dispersion conversion of hypericin by noncanonically structured DNA and a fluorescent  $\text{Ba}^{2+}$  sensor. *Sens. Actuators, B* **2017**, *247*, 19–25; (d) Sivakumar, K.; Parameswari, M.; Stalin, T. Etodolac:  $\beta$ -cyclodextrin inclusion complex as a novel fluorescent chemosensor probe for  $\text{Ba}^{2+}$ . *J. Carbohyd. Chem.* **2016**, *35*, 118–130.
- (10) (a) Ji, H. F.; Yang, Y.; Xu, X.; Brown, G. A calixarene based fluorescent  $\text{Sr}^{2+}$  and  $\text{Ca}^{2+}$  probe. *Org. Biomol. Chem.* **2006**, *4*, 770–772; (b) Banerjee, T.; Suresh, M.; Ghosh, H. N.; Das, A. Competitive binding of  $\text{Ba}^{2+}$  and  $\text{Sr}^{2+}$  to 18-Crown-6 in a receptor with a 1-methoxyanthraquinone analogue as the other binding site. *Eur. J. Inorg. Chem.* **2011**, 4680–4690; (c) Sutariya, P. G.; Pandya, A.; Modi, N. R.; Menon, S. K. A highly efficient PET switch on-off-on fluorescence receptor based on calix[4]arene for the selective recognition of  $\text{Cd}^{2+}$  and  $\text{Sr}^{2+}$ . *Analyst* **2013**, *138*, 2244–2248; (d) Kaur, S.; Kaur, A.; Kaur, N.; Singh, N. Development of chemosensor for  $\text{Sr}^{2+}$  using organic nanoparticles: application of sensor in product analysis for oral care. *Org. Biomol. Chem.* **2014**, *12*, 8230–8238; (e) Kaur, A.; Kaur, G.; Singh, A.; Singh, N.; Kaur, N. Polyamine based ratiometric fluorescent chemosensor for strontium metal ion in aqueous medium: application in tap water, river water, and in oral care. *ACS. Sustain. Chem. Eng.* **2016**, *4*, 94–101.
- (11) (a) Nimse, S. B.; Kim, T. Biological applications of functionalized calixarenes. *Chem. Soc. Rev.* **2013**, *42*, 366–386; (b) Kumar, R.; Sharma, A.; Singh, H.; Suating, P.; Kim, H. S.; Sunwoo, K.; Shim, I.; Gibb, B. C.; Kim, J. S. Revisiting Fluorescent Calixarenes: From Molecular Sensors to Smart Materials. *Chem. Rev.* **2019**, *119*, 9657–9721.
- (12) (a) Sreedevi, P.; Nair, J. B.; Preethanuj, P.; Jeeja, B. S.; Suresh, C. H.; Maiti, K. K.; Varma, R. L. Calix[4]arene based redox sensitive molecular probe for SERS guided recognition of labile iron pool in tumor cells. *Anal. Chem.* **2018**, *90*, 7148–7153; (b) Wang, K.; Guo, D.; Jiang, B.; Liu, Y. Highly selective fluorescent chemosensor for  $\text{Na}^{+}$  based on pyrene-modified calix[4]arene derivative. *Sci. China. Ser. B* **2009**, *52*, 513–517; (c) Segura, M.; Bricoli, B.; Casnati, A.; Munoz, E. M.; F. Sansone, Ungaro, R.; Vicent, C. A prototype calix[4]arene-based receptor for carbohydrate recognition containing peptide and phosphate binding groups. *J. Org. Chem.* **2003**, *68*, 6296–6303.
- (13) Li, H.; Zhan, J.; Chen, M.; Tian, D.; Zou, Z. Metal ions recognition by 1,2,3-triazolium calix[4]arene esters synthesized via click chemistry. *J. Incl. Phenom. Macrocycl. Chem.* **2010**, *66*, 43–47.
- (14) Tsien, R. Y. A non-disruptive technique for loading calcium buffers and indicators into cells. *Nature* **1981**, *290*, 527–528.
- (15) Kim, H. M.; Kim, B. R.; Hong, J. H.; Park, J.-S.; Lee, K. J.; Cho, B. R. A two-photon fluorescent probe for calcium waves in living tissue. *Angew. Chem. Int. Ed.* **2007**, *46*, 7445–7448.
- (16) Slater, J. C. Atomic Radii in Crystals. *J. Chem. Phys.* **1964**, *41*, 3199–3204.
- (17) (a) Zhang, H.; Sun, T.; Ruan, Q.; Zhao, J. L.; Mu, L.; Zeng, X.; Jin, Z.; Su, S.; Luo, Q.; Yan, Y.; Redshaw, C. A multifunctional tripodal fluorescent probe for the recognition of  $\text{Cr}^{3+}$ ,  $\text{Al}^{3+}$ ,  $\text{Zn}^{2+}$  and

F<sup>-</sup> with controllable ESIPT processes. *Dyes. Pigments.* **2019**, *162*, 257–265; (b) Ruan, Q.; Mu, L.; Zeng, X.; Zhao, J. L.; Zeng, L.; Chen, Z. M.; Yang, C.; Wei, G.; Redshaw, C. A three-dimensional (time, wavelength and intensity) functioning fluorescent probe for the selective recognition/discrimination of Cu<sup>2+</sup>, Hg<sup>2+</sup>, Fe<sup>3+</sup> and F<sup>-</sup> ions. *Dalton Trans.* **2018**, *47*, 3674–3678.

(18) Thordarson, P. Determining association constants from titration experiments in supramolecular chemistry. *Chem. Soc. Rev.* **2011**, *40*, 1305–1323.

(19) Xin, F.; Tian, Y.; Gao, C.; Guo, B.; Wu, Y.; Zhao, J.; Jing, J.; Zhang, X. A two-photon fluorescent probe for basal formaldehyde imaging in zebrafish and visualization of mitochondrial damage induced by FA stress. *Analyst* **2019**, *144*, 2297–2303.

(20) Three-day-old zebrafish were incubated with various concentration of sensor **L** (1 μM, 2 μM, 3 μM, 4 μM, 5 μM, 10 μM, 15 μM, 20 μM) in 24-well flat-bottomed plates (10 zebrafish in each well) at room temperature. When the concentration of sensor **L** exceeded 5 μM, the zebrafish were dead within 10 min.; when the concentration of sensor **L** was 4 μM, only a few zebrafish died in 10 min., most survived longer. However, when the concentration of sensor **L** was 3 μM or lower, all the zebrafish survived for more than 4 hours, and more than half zebrafish survived for several days. Combining the incubation time and the imaging quality, we selected the best conditions for the zebrafish fluorescence imaging experiments to be three-day-old zebrafish incubated with the 3 μM sensor **L** for 30 min. at room temperature.

(21) (a) Singh, D. P.; Dwivedi, R.; Singh, A. K.; Koch, B.; Singh, P.; Singh, V. P. A dihydrazone based “turn-on” fluorescent probe for selective determination of Al<sup>3+</sup> ions in aqueous ethanol. *Sens. Actuators, B.* **2017**, *238*, 128–137; (b) Wu, Y. T.; Zhao, J. -L.; Mu, L.; Zeng, X.; Wei, G.; Redshaw C.; Jin, Z. A 2-Styryl-1,8-naphthyridine derivative as a versatile fluorescent probe for the selective recognition of Hg<sup>2+</sup>, Ag<sup>+</sup> and F<sup>-</sup> ions by tuning the solvent. *Sens. Actuators, B.* **2017**, *252*, 1089–1097.

(22) (a) Neel A. J.; Hilton M. J.; Sigman M. S.; Toste F. D. Exploiting non-covalent π interactions for catalyst design. *Nature* **2017**, *543*, 637–646; (b) Liao J.-Z.; Chang J.-F.; Meng L.; Zhang H.-L.; Wang S.-S.; Lu C.-Z. Lone pair–π interaction-induced generation of photochromic coordination networks with photoswitchable conductance. *Chem. Commun.* **2017**, *53*, 9701–9704; (c) Wang Y.; Pigeon P.; Top S.; García J. S.; Troufflard C.; Ciofini I.; McGlinchey M. J.; Jaouen G. Atypical lone pair–π interaction with quinone methides in a series of imido-ferrociphenol anticancer drug candidates. *Angew. Chem. Int. Ed.* **2019**, *58*, 8421–8425; (d) Mooibroek T. J.; Gamez P.; Reedijk J. Lone pair–π interactions: a new supramolecular bond? *CrystEngComm* **2008**, *10*, 1501–1515.

# Table of Contents

A molecular tweezers like calix[4]arene chemosensor exhibits excellent selective recognition and discrimination towards  $\text{Ca}^{2+}$ ,  $\text{Sr}^{2+}$  &  $\text{Ba}^{2+}$  via a rare synergistic effect. It further exhibits an excellent sensing and imaging capability in living cells and in Zebrafish.

